IEEE Access
Multidisciplinary | Rapid Review | Open Access Journal

Received November 6, 2018, accepted November 28, 2018, date of publication December 5, 2018,
date of current version December 31, 2018.

Digital Object Identifier 10.1109/ACCESS.2018.2884946

A Dual Linearly Polarized End-Fire Antenna Array for the 5G Applications

AO LI[1], KWAI-MAN LUK[1], (Fellow, IEEE), AND YUJIAN LI[2], (Member, IEEE)
[1]State Key Laboratory of Terahertz and Millimeter Wave, City University of Hong Kong, Hong Kong
[2]Institute of Lightwave Technology, Beijing Jiaotong University, Beijing 100044, China

Corresponding author: Ao Li (aoli26-c@my.cityu.edu.hk)

This work was supported by the Research Grant Council of Hong Kong, China, under Project 9042377 (CityU 11277116).

ABSTRACT A dual linearly polarized antenna array with end-fire radiation of the 60-GHz band is proposed by combining two types of magneto-electric dipoles (ME-dipole), which operate in vertical polarization (V-pol) and horizontal polarization (H-pol), respectively. Based on the substrate integrated waveguide structure, two kinds of ME-dipole are placed closely by sharing the same metallic post wall between them, achieving an element space of $0.77\lambda_0$. Besides, mutual coupling between the close elements is numerically analyzed and then suppressed by making modifications to the antenna structure. The proposed dual-polarized element achieves bandwidths of 26% and 32% ($|S_{11}| < -14$ dB) for the V-pol and H-pol, respectively. A 1×8 element array is designed, fabricated, and measured. Good agreement is achieved between the measurement and simulation. For the V-pol excitation, a bandwidth of 21% is obtained and gain is up to 16.1 dB. For the H-pol excitation, the bandwidth is 18% and peak gain is 15.1 dB. Radiation patterns are stable over the operating frequencies with cross polarizations below -30 dB for both polarizations. The port isolation is very high above 45 dB. With all these advantages of dual polarization, end-fire radiation, stable gain, and high port isolation, the proposed array is a potential candidate for the future 5G applications.

INDEX TERMS Dual linear polarization, end-fire radiation, high isolation, magneto-electric dipole (ME-dipole), substrate integrated waveguide (SIW).

I. INTRODUCTION

Over the past decade, increasing attention has been drawn to the 5th generation (5G) mobile communication, which aims to realize higher data rate, reduced latency, larger system capacity and massive device connectivity. Recently, different countries have identified the lower frequency bands (below 6 GHz) for the 5G communications, including 600/ 3100-3550/ 3700-4200 MHz of the United States, 700/ 3400-3800MHz of Europe, 3300-3600/ 4800-5000 MHz of China and 3500 MHz of South Korea. However, to the best of the authors' knowledge, the higher frequency bands are still under trial. Several millimeter wave (mm-wave) bands including 28-GHz, 38-GHz and 60-GHz are believed to be potential candidates for the upper frequency band of 5G thereby being investigated widely. The 60-GHz band owns great advantages because of the free license and wide bandwidth available for multi-gigabit data rate [1]. However, higher frequency means higher transmission loss, so from the perspective of antenna [2], [3], high performance antenna arrays are required for the upper frequency band of 5G.

Various antenna arrays working at the 60-GHz band or other mm-wave bands have been reported [4]–[10]. These arrays share the same characteristic of the broadside radiation, while the end-fire array can provide some flexibility in some practical applications therefore also being needed. Besides, most reported works are on designing with the single polarization, which is not so attractive comparing with the dual polarization because the dual polarization can provide more reliability and enhance the capacity for the 5G communications [4]. Unfortunately, antenna arrays with features of both end-fire radiation and dual polarization are still very rare in mm-wave bands.

Typical antennas with end-fire radiation, including horn antenna, Yagi-Uda antenna, tapered slot antenna, log-periodic antenna, *etc.* have wideband properties but meantime behave unstable radiation performances with the frequency varying [11]. These antennas also have a relatively large size in the longitudinal direction. A few end-fire arrays have been reported at mm-wave bands by using tapered slot antennas [12]–[14]. References [15] and [16] reported end-fire

antenna arrays in the form of dielectric rod and dielectric resonator respectively, which however are not easy for integration.

Both dual linearly polarized [17]–[19] and dual circularly polarized [20], [21] arrays have been reported in mm-wave bands recently, but still with a broadside radiation. Generally, two feed networks are required for two polarizations and good isolation between the two input ports is crucial for dual-polarized arrays. In [20], the feed network is shared by two polarizations and two 3-dB hybrid couplers are used for the polarization switching. However, principally this method can only be used for the dual circular polarization case and the array will suffer from a poor port isolation.

In [22], an excellent dual-polarized end-fire phased array was realized for mm-wave radar by using a compact L-shaped horn antenna as the element. An active phase-tuning feed network was also proposed and validated well. However, the port isolation is not good enough because of the shared asymmetrical L-shape aperture. Moreover, the complex network causes a large insertion loss and the used stereo-lithography fabrication technique is not so cost friendly. In [23], a dual-polarized end-fire array was realized using quasi Yagi-Uda antennas for MIMO terminals at Ka-band. A 1×4 array was fabricated by the printed circuit board (PCB) technology. However, the feature of dual polarization was demonstrated by two separated prototypes without a combined feed solution. Recently in [24], a dual circularly polarized end-fire antenna array was presented by inserting a polarizer in the two-layer open-end substrate integrated waveguide (SIW). The array also achieved multi-beam performance by using the butler matrix.

The coauthor's group have already accomplished some works of dual-polarized [25], [26] and end-fire [27], [28] antenna arrays at the 60-GHz band. In the conference paper of [29] Li and Luk reported some initial works of a dual linearly polarized end-fire antenna array. In this paper, the array in [29] is further studied. The detail design guide line and complete experimental demonstration of the dual linearly polarized end-fire antenna array are presented. The proposed array begins from two types of end-fire magneto-electric dipole (ME-dipole) in [27] and [28], which provide a solution for the vertical polarization (V-pol) and horizontal polarization (H-pol) respectively. In order to guarantee the potential beam scanning property and avoid the grating lobes, these two kinds of elements are placed closely by sharing a same metallic post wall between them. However, the mutual coupling is found among the tight elements, so crucial modifications including the separation slot and extended plane waveguide are employed to suppress the mutual coupling. Besides, the corrugated substrate is loaded in front of the open-end SIW to improve the impedance matching for both V-pol and H-pol excitation simultaneously. In addition, two feed networks are designed to excite the V-pol and H-pol separately for the good port isolation. To complete the feed networks, a wideband Y-junction is proposed to guarantee close distance between output ports and a back-to-back coupling transition between the 1st and 3rd substrates is also presented. A prototype is fabricated and good performances are demonstrated through measurement.

This paper is organized as follows. The detailed geometry and design procedure of the dual-polarized element antenna are presented in section II. Simulated and measured results of the proposed 1×8 array are illustrated and compared in section III. And a conclusion is given in section IV.

II. DUAL-POLARIZED END-FIRE ME-DIPOLE

The general operating principle of ME-dipole is to excite a pair of orthogonal magnetic dipole (M-dipole) and electric dipole (E-dipole) with equal amplitudes simultaneously. In this paper, for the V-pol ME-dipole as shown in Figure 1 (a), the conventional open-end SIW operates as the M-dipole and the four metallic vias in the lower and upper substrates operate as the E-dipole. For the H-pol ME-dipole as shown in Figure 1 (b), the vertical open-end SIW operates as the M-dipole and the four small patches in the middle two copper layers play the role of E-dipole. More design details have been introduced in [27] and [28]. So this section mainly focuses on the design considerations and modifications preparing for the dual-polarized array configuration.

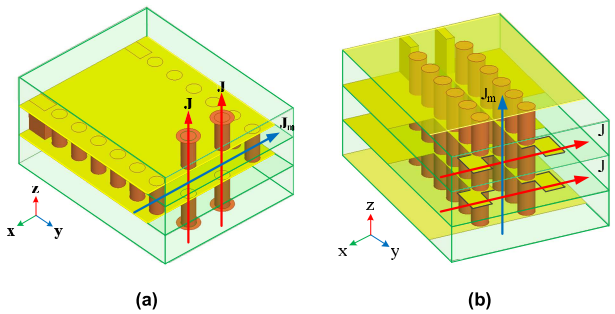

FIGURE 1. Structure of end-fire ME-dipole. (a) V-pol ME-dipole and (b) H-pol one. Reproduced from [27] and [28].

Figure 2 shows the structure evolution and 3D view of the proposed dual-polarized ME-dipole. Both the V-pol and H-pol ME-dipole are constructed by three stacked dielectric substrates with a thickness of 0.787 mm each. With a width of 2.83 mm and 1 mm for the V-pol element and H-pol element respectively, the whole element space is 3.83 mm, 0.77 λ_0 of 60 GHz, which is suitable for array design without significant grating lobes. As for the SIW configuration, the via holes are 0.35 mm in diameter and 0.6 mm in separation. To take the mutual coupling among elements in the array into account, the 'master' and 'slave' boundaries are assumed to the dual-polarized element in x-axis in order to create a periodic boundary condition [6].

Firstly, V-pol ME-dipole and H-pol ME-dipole are tightly integrated together by sharing a same post wall between them as shown in Figure 2 (b), but it is found that the small patches of the H-pol element connect with the V-pol element. So the V-pol one is shorten slightly, leaving a slot for separation as shown in Figure 2 (c). However, these patches are still located

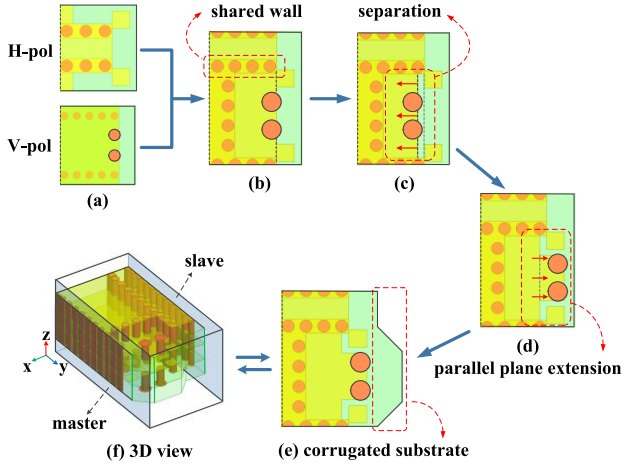

FIGURE 2. Design procedure of dual-polarized ME-dipole element. The element is assigned with periodic boundaries for the simulation.

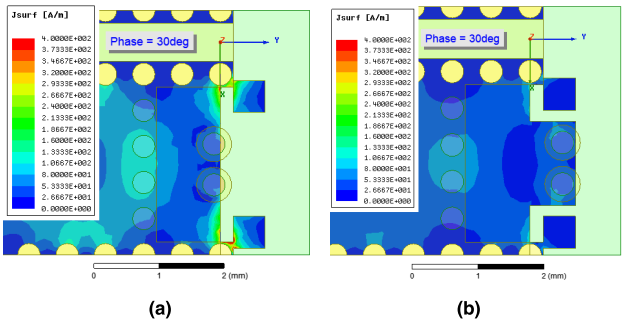

FIGURE 3. Current distribution of middle layer at 60 GHz when V-pol element is excited. (a) before and (b) after extending radiation aperture of V-pol element.

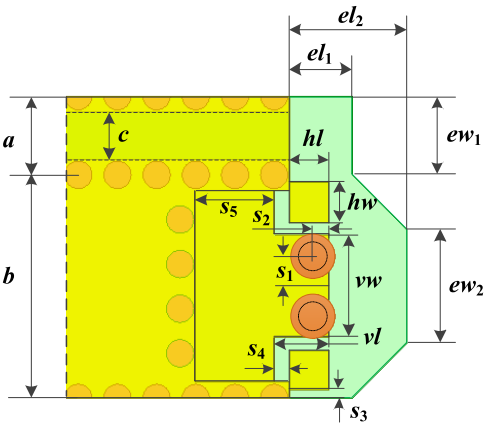

FIGURE 4. Detailed geometry of modified dual-polarized ME-dipole in top view, corrugated dielectric extension is employed to improve impedance matching of both polarizations. Dimensions are $a = 1$, $b = 2.83$, c=0.6, hl=0.5, hw=0.5, vw=1.3, vl=0.7, s_1 =0.32, $s_2 = 0.2$, $s_3 = 0.08$, $s_4 = 0.2$, $s_5 = 1$, $ew_1 = 1$, $el_1 = 0.96$, $ew_2 = 1.43$, $el_2 = 1.66$, all in mm.

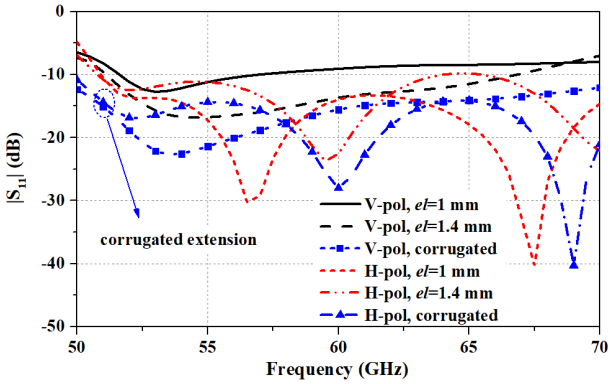

FIGURE 5. Comparison of reflection coefficient among elements with different dielectric substrate extensions, uniform extension of 1mm, 1.4 mm, and the corrugated extension.

in front of the aperture of the V-pol ME-dipole so that they will distort the electric/magnetic-field distribution because of the blocking and mutual coupling effects. Simulation proves that the radiation pattern of the V-pol ME-dipole gets very unstable and asymmetrical after integrated with the H-pol ME-dipole. Thus, the open-end SIW for V-pol is extended by a length of parallel plane waveguide and the E-dipole vias are also moved a distance forward as shown in Figure 2 (d). To illustrate this changing, the surface current distributions of the middle metal layer at 60 GHz before/after the modification are given in Figure 3. Before the modification, the small patches attract a large amount of current so that the amplitude balance between M-dipole and E-dipole of the V-pol element are broken. After the modification, the current in the small patches decreases remarkably. By carefully adjusting other geometric parameters, the V-pol ME-dipole can rebuild the amplitude balance thereby keeping stable radiation performance and pure polarization. Fortunately, the radiation performance of the H-pol ME-dipole is not affected by the blocking or mutual coupling effects. So after modifying the V-pol ME-dipole, the H-pol ME-dipole maintains unchanged. Then, the substrate is extended in a corrugate form to improve the impedance matching as shown in Figure 2 (e).

A uniform extension is investigated in the beginning. As shown in Figure 5, with the extension length '*el*' changing from 1 mm to 1.4 mm, the reflection coefficient of the V-pol excitation decreases while that of the H-pol excitation increases, which means the two types of ME-dipole prefer different extension lengths for good impedance matching. So there must be a tradeoff between the two polarizations if using a uniform extension. Instead, as shown in Figure 4, a corrugated extension is employed in front of the proposed dual-polarized element. Simulated results in Figure 5 illustrate that a significant improvement is obtained by the corrugated substrate extension. The bandwidths of the V-pol and H-pol are 26% (from 50.6 to 65.4 GHz) and 32% (from 50.9 to 70 GHZ) respectively for $|S_{11}| < -14$ dB. The final geometry of the corrugated extension can be easily determined by tuning the related parameters especially 'el_1' and 'el_2'. The final dimensions are given in the caption of Figure 4.

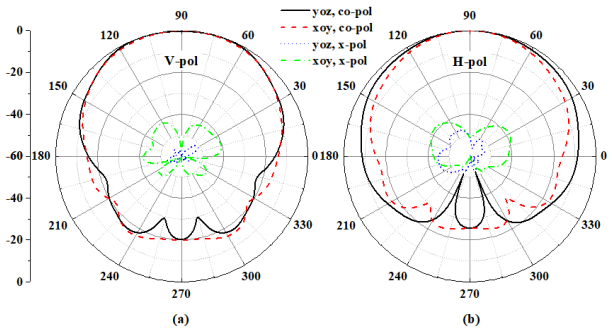

FIGURE 6. Radiation patterns of the proposed dual-polarized element at the center frequency of 60 GHz. (a) V-pol and (b) H-pol.

Figure 6 illustrates the radiation patterns at the center frequency of 60 GHz. Symmetrical radiation patterns are attained except a slightly narrower beam in the E-plane (xoy plane) of the H-pol operation. The cross polarization is almost less than −40 dB and front-to-back ratio is over 20 dB for both polarizations. The simulated gain and front-to-back ratio versus frequency are given in Figure 7. Within the band from 55 to 65 GHz, the H-pol radiation exhibits a stable gain, which ranges from 6.6 to 7.1 dB. While the V-pol radiation meets a larger gain variation of 2 dB and a higher average gain. The V-pol radiation also has a larger fluctuation of front-to-back ratio which is slightly smaller at lower frequencies but still over 18 dB at 55 GHz. In fact, the small patches of the H-pol element still have some negative influences on the performance of the V-pol element so a tradeoff exists in parameter tuning. Table 1 summarizes the performance of the proposed dual-polarized ME-dipole.

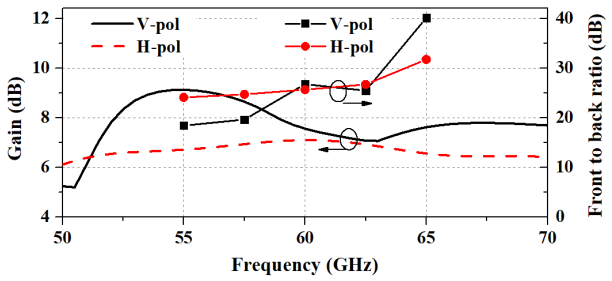

FIGURE 7. Simulated gain and front-to-back ratio versus frequency.

TABLE 1. Performance of proposed dual-polarized ME-Dipole.

Pol.	Bandwidth ($\|S_{11}\|$<-14 dB)	Gain	Front-to-Back Ratio	x-pol
V-pol	26%	>7.0 dB	>18 dB	<-40 dB
H-pol	32%	>6.6 dB	>24 dB	<-40 dB

III. DUAL LINEARLY POLARIZED ANTENNA ARRAY

This section presents a 1×8 dual-polarized antenna array. Two equal 8-way SIW feed networks are built to feed the element antennas. The whole configuration of the proposed array and two components are introduced. Commercial electromagnetic simulator HFSS was used for the simulation.

A. 1 × 8 ANTENNA ARRAY

Figure 8 shows the 3D view and the energy flow within different layers of the proposed antenna array. Eight dual-polarized ME-dipole elements presented in section II are arranged closely as the radiators. Two separated feed networks are integrated together to excite the expected V-pol and H-pol respectively.

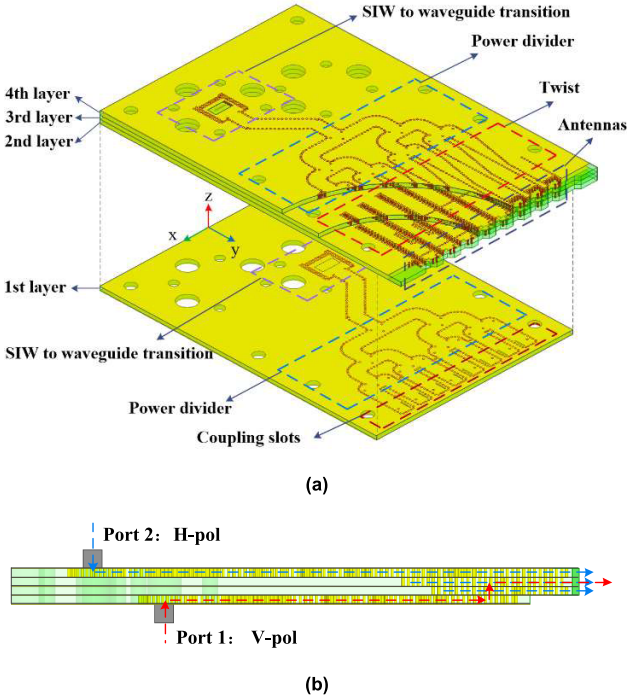

FIGURE 8. Whole structure of the proposed dual-polarized antenna array. (a) 3D view with illustration of array's configuration, and (b) side view with illustration of energy flows when array operates at V-pol or H-pol.

In the design procedure of feed networks, firstly an equal 8-way SIW power divider is built. Secondly, a SIW-to-waveguide transition is connected with the 8-way power divider because the standard waveguide adapter of WR-15 (50-75 GHz) will be used to inject the electromagnetic wave in the measurement. The two input ports are placed on different sides with a little shift from the longitudinal axis considering the installation of waveguide adapters. Finally, a SIW coupling transition between the 1st and 3rd substrate layers for the V-pol and a SIW polarization twist for the H-pol are introduced to connect the power dividers with the radiators therefore completing the energy flow routes.

For the 8-way power divider, three T-dividers and four Y-dividers are contained. As shown in Figure 9 (a), it is a conventional method to use three metallic posts to achieve broadband impedance matching for the SIW T-divider. Round edges are chosen for bends to further improve the impedance matching. To guarantee a close distance between adjacent outputs for arraying, a modified Y-divider is proposed as

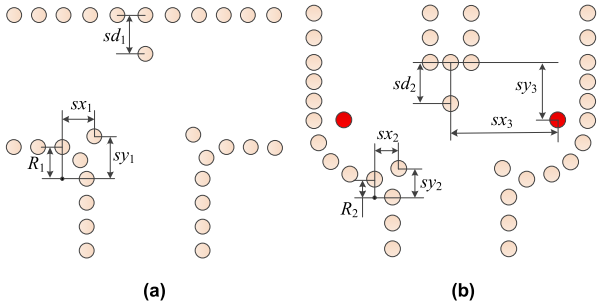

FIGURE 9. Geometry of SIW power divider in top view. (a) T-divider and (b) modified Y-divider. Dimensions are $R_1 = 0.6$, $R_2 = 0.5$, $sx_1 = 0.8$, $sy_1 = 0.9$, $sd_1 = 1$, $sx_2 = 0.65$, $sy_2 = 0.75$, $sd_2 = 1$, $sx_3 = 2.6$, $sy_3 = 1.35$, all in mm.

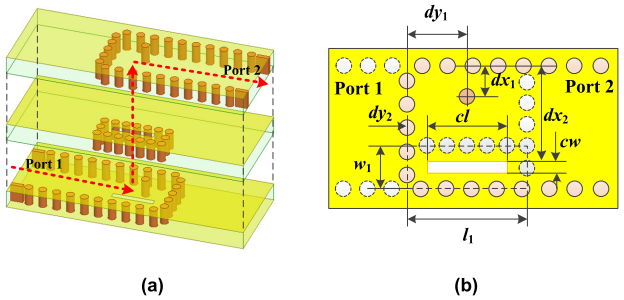

FIGURE 11. Back-to-Back SIW coupling transition between different substrate layers for V-pol feed network. (a) 3-D view with illustration of power flow and (b) detailed geometry of the proposed structure. Dimensions are $dx_1 = 0.72$, $dy_1 = 1.51$, $dx_2 = 2.22$, $dy_2 = 0.47$, cl=2.08, cw=0.2, $l_1 = 2.8$, $w_1 = 1$, all in mm.

the last stage of the 8-way power divider. Apart from the three metallic posts like in the T-divider, two more posts (the red ones) are employed to adjust the impedance matching as shown in Figure 9 (b). Detailed dimensions of both the T-divider and modified Y-divider are listed in the caption of Figure 9. Simulated reflection coefficients are given in Figure 10. The T-divider shows a bandwidth of 42% (48∼73.5 GHz) for $|S_{11}| < -15$ dB while the Y-divider performs badly in matching. By adding the two extra metallic posts, the modified Y-divider yields significantly matching improvement, realizing a bandwidth of 41% (48∼72.5 GHz). The performance of the whole 8-way divider is given later in the same subsection.

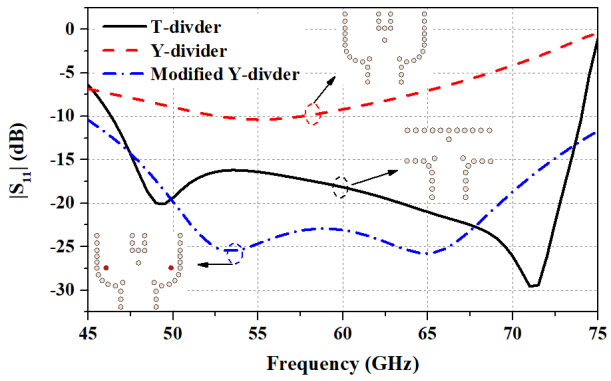

FIGURE 10. Reflection coefficient of different SIW dividers.

For the SIW coupling transition between the 1st and 3rd substrate layers, a back-to-back coupling structure is the proposed as shown in Figure 11. The electromagnetic energy flows from the 1st substrate to 3rd substrate through two coupling slots which are etched on copper layers between adjacent substrates with a distance of offset from the longitudinal axis. The dimension of the coupling slot determines the resonant frequencies and an extra post is employed to improve the impedance matching. The 2nd substrate layer contains a series of posts to form a short vertical waveguide for the energy transmission. Final dimensions of the proposed coupling transition are listed in the caption of Figure 11.

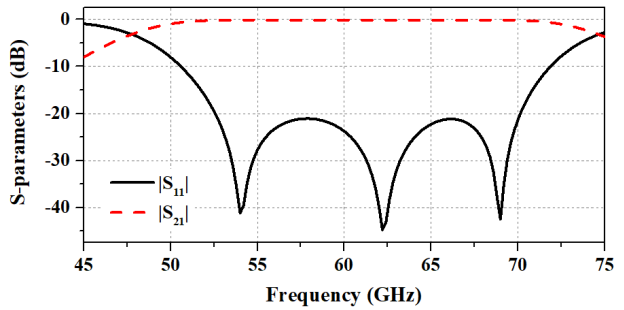

FIGURE 12. Simulated S-parameters of the Back-to-Back SIW transition structure between different layers for the V-pol feed network.

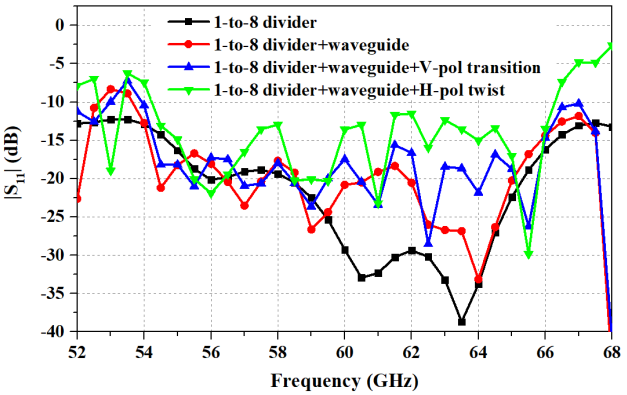

FIGURE 13. Reflection coefficients of different feed networks.

S-parameters of the back-to-back coupling transition are shown in Figure 12. A bandwidth of 29% (51-68.5 GHz) is achieved for $|S_{11}| < -15$ dB and the maximal insertion loss is only 0.3 dB in the operating band.

As for another two essential components for the whole feed networks, namely the SIW-to-waveguide transition and the SIW polarization twist for H-pol. The authors made reference to [10] and [28] to complete the design, and interested readers can find detailed guidelines in these two literatures. Geometries have been slightly tuned for the impedance matching of the proposed networks in this paper.

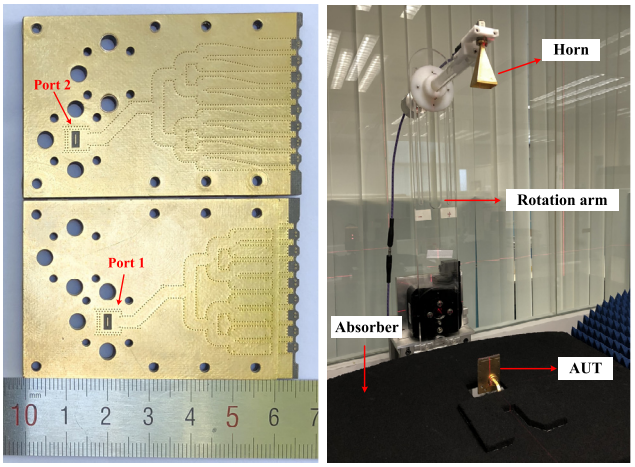

FIGURE 14. Measurement for the proposed array. (a) prototype with top and bottom view, and (b) radiation pattern measurement setup under the far-field test system.

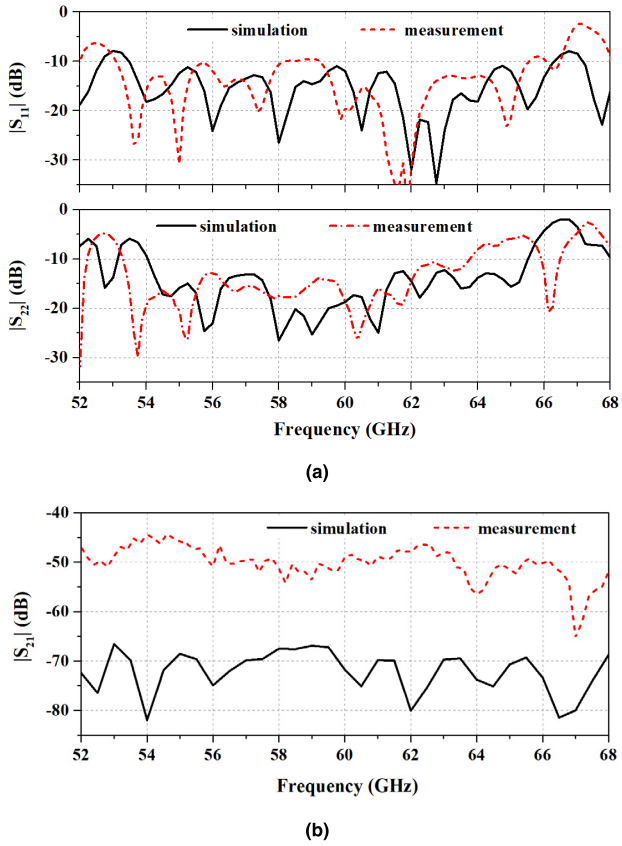

FIGURE 15. Simulated and measured S-parameters: (a) $|S_{11}|$ & $|S_{22}|$, and (b) $|S_{21}|$.

Figure 13 gives the reflection coefficients of the network in different forms. During the design of the network, the authors aimed at achieving a goal that $|S_{11}|$ is less than -15 dB over a wide frequency band. Simulated results demonstrate that the reflection coefficient almost keeps below -15 dB

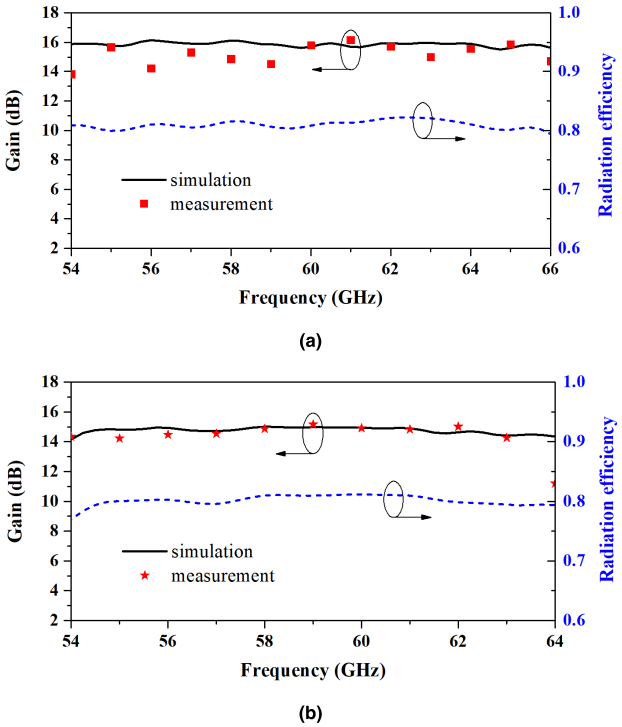

FIGURE 16. Comparison between simulated and measured gain, as well as the simulated radiation efficiency of the proposed dual-polarized antenna array: (a) port 1 excitation, i.e. V-pol radiation, and (b) port 2 excitation, i.e. H-pol radiation.

from 54 to 66 GHz except for the complete H-pol network where -12 dB has been reached at some frequencies. However, the whole array also exhibits good impedance matching for the H-pol radiation because of enough margin achieved by the element antenna. Simulated and measured results of the whole array are illustrated and compared in following subsection.

B. EXPERIMENTAL RESULTS

A prototype of the proposed dual-polarized antenna array was fabricated by the cost-effective PCB technology as shown in Figure 14 (a). The substrates used are commercial Rogers 5880 (with $\varepsilon = 2.2$, $\tan\delta = 0.0009$, and a thickness of 0.787 mm), covered by copper layers(18 um in thickness) on both sides. The prototype consists of four substrates which were fabricated separately and then bonded together using Rogers COOLSPAN Thermally and Electrically Conductive Adhesive (TECA) films [9]. The TECA film, which is 0.05 mm in thickness, can eliminate the possible air gaps between adjacent substrates. The overall size of the prototype is 66 mm $\times$ 43 mm $\times$ 3.3 mm. In the experiment, S-parameters were measured by an Anritsu MS4647B Vector Network Analyzer (VNA) with a 3743A mm-wave modulate. The radiation patterns were measured by a far-field test system as shown in Fig 14 (b) and the gain was attained by comparing the prototype with a standard-gain horn.

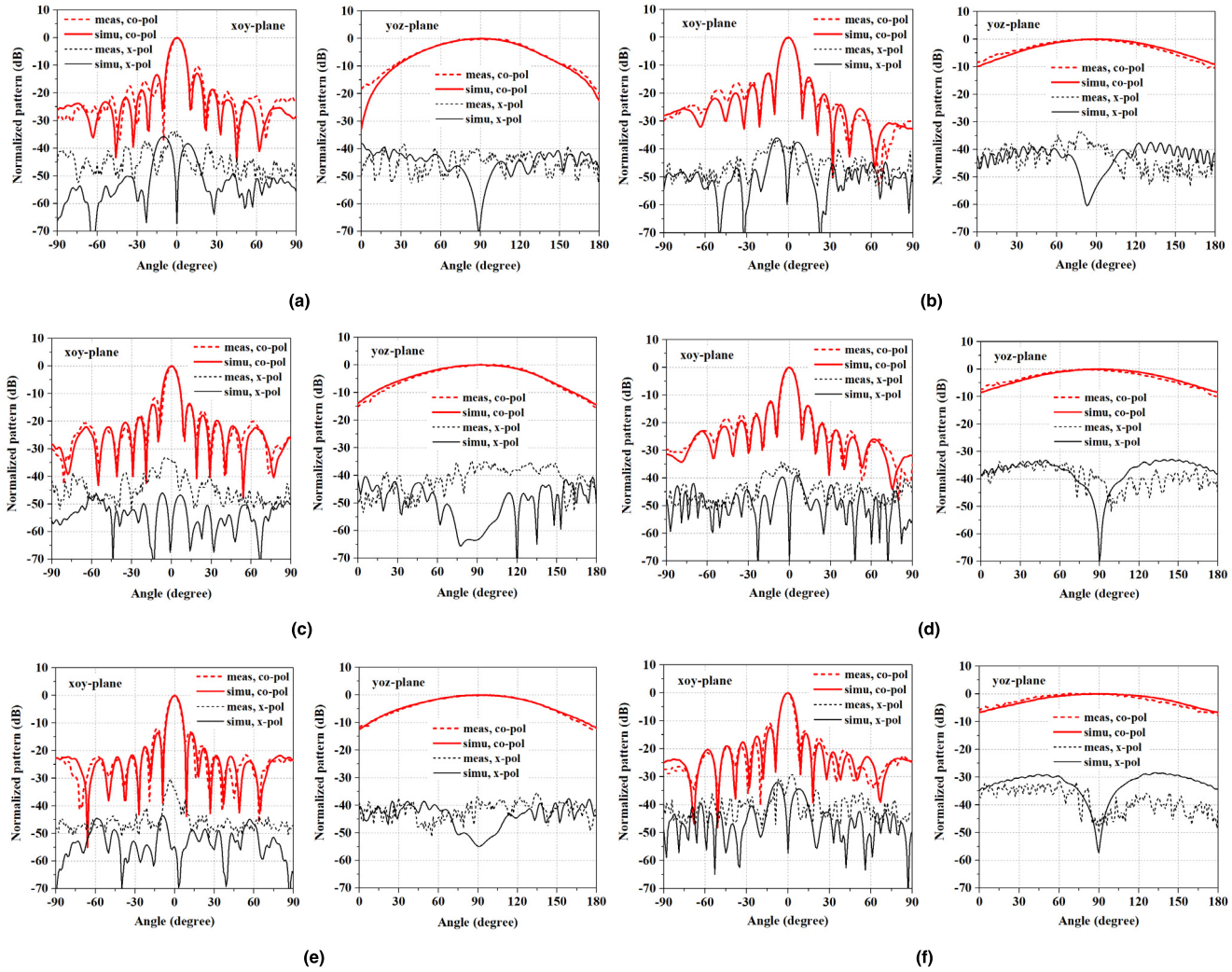

FIGURE 17. Radiation patterns of proposed dual-polarized antenna array at different frequencies: 55 GHz with (a) port 1 and (b) port 2 excitation; 60 GHz with (c) port 1 and (d) port 2 excitation; 64 GHz with (e) port 1 and (f) port 2 excitation. (a) 55 GHz, port 1. (b) 55 GHz, port 2. (c) 60 GHz, port 1. (d) 60 GHz, port 2. (e) 64 GHz, port 1. (f) 64 GHz, port 2.

Measured and simulated S-parameters of the proposed array are given in Figure 15 and a good agreement is achieved. Port 1 and Port 2 are input ports for the V-pol and H-pol excitation respectively. For the V-pol excitation, an operation bandwidth ($|S_{11}| < -10$ dB) of 21% (53.1∼65.5 GHz) is obtained in measurement. $|S_{11}|$ is about −9.6 dB near 59 GHz, slightly over −10 dB but acceptable. There exists a small frequency shift of 0.5 GHz between measured and simulated results. For the H-pol excitation, the measured bandwidth is 18% (53.3∼63.7 GHz), observing a similar frequency shift of 0.8 GHz, which however is still acceptable. The matching gets worse at upper frequency region for the prototype, which results in a relatively narrower bandwidth. The difference between measurement and simulation should be mainly caused by (1) fabrication tolerances, especially for the corrugated substrate extension, (2) parameter differences of the substrate including permittivity and copper layer thickness, (3) tiny misalignment of substrates and bonding films. The isolation between the two ports is evaluated by $|S_{21}|$ which is given in Figure 15 (b). Note that $|S_{21}|$ seems extremely small so the authors tried to reduce the convergence criteria (setting of HFSS) in order to get an accurate result during the simulation. But the computer resource is limit so that "Maximum Delta-S=0.003 (−50 dB)" was set as the final convergence criteria. It comes out that the simulated $|S_{21}|$ could be weakly accurate since it is below the convergence tolerance. However, the result can still prove that simulated $|S_{21}|$ is smaller than −50 dB at least therefore being given here as a reference. The measured value is below −45 dB. The difference seems large but it may happen easily since $|S_{21}|$ is truly extremely small. The reasons could be the tiny errors from fabrication and alignment, even the natural noise during the measurement.

The gain of the proposed array was obtained by comparing the prototype with a standard-gain horn as mentioned above. Figure 16 gives measured and simulated gains of the array,

TABLE 2. Comparison between proposed and reported dual-polarized antenna arrays.

Ref.	Antenna array	Polarization	Radiation	Bandwidth (VSWR<2)	Max. gain (dB)	Max. rad. efficiency	Isolation (dB)	Fabrication
[18]	16×16 (Slot)	Dual linear	Broadside	6.8% (VSWR<1.5)	32	80%	50	Diffusion bonding
[19]	8×8 (Slot)	Dual linear	Broadside	6.2%	22.3	84.5%	25	Metal milling
[20]	8×8 (Patch)	Dual circular	Broadside	8.9% (AR<3dB)	19.35	NA	19	PCB
[21]	2×2 (Patch)	Dual circular	Broadside	17% (AR<3dB)	17.85	72%	20	PCB
[22]	1×10 (Horn)	Dual linear	End-fire	16%	15.6	17.8%	15	Stereo-lithography
[23]	1×4 (Quasi-Yagi)	Dual linear	End-fire	25%	11	80%	20	PCB
[24]	1×4 (Open-end SIW)	Dual circular	End-fire	22.5% (AR<3dB)	12.8	51.6%	15	PCB
This work	1×8 (ME-dipole)	Dual linear	End-fire	21%	16.1	82%*	45 / 65*	PCB

'' the value is a simulated result.*

as well as the simulated radiation efficiency. Good agreement is achieved between the measurement and simulation. For the V-pol radiation, the measured gain experiences a peak value of 16.1 dB and a variation of 2.3 dB within the operation band from 54 to 66 GHz. For the H-pol radiation, the gain sees a slightly smaller peak value of 15.1 dB but meantime a smaller variation of 0.9 dB within the operating band from 54 to 63 GHz. The difference between the V-pol and H-pol radiation is mainly determined by the radiation performance of the elements as investigated in section II.

Measured and simulated radiation patterns of both V-pol and H-pol are given in Figure 17. Three frequencies, 55 GHz, 60 GHz, and 64 GHz, are chosen to illustrate the radiation performance of the array prototype. All the radiation patterns presented demonstrate a great agreement between the measurement and simulation. The radiation pattern is very stable over the frequency band for both polarizations. The array obtains a narrow main-beam (around 8 degrees for 3-dB beamwidth) in xoy-plane because of the array arrangement. The side-lobe keeps below −10 dB. The cross polarization is below −30 dB due to the excellent performance of the ME-dipole.

C. COMPARISON WITH SOME REPORTED WORKS

Table 2 summarizes the performances and configurations of the proposed antenna array and reported mm-wave dual-polarized antenna arrays for comparison. As mentioned above, an antenna array with features of both dual polarization and end-fire radiation is still rare, so only three cases are listed and the others are broadside ones. In term of operating bandwidth, the proposed design achieves a relatively good performance of 21%, which is slightly less than those of [23] and [24] mainly because of the bandwidth limit of a larger feed network. Due to the low-loss substrate and SIW structure, the radiation efficiency of this work is comparable to those high efficiency antenna arrays in [18] and [19]. Note that the conductive adhesive film used is crucial to guarantee the high radiation efficiency performance because possible air gaps between adjacent substrates can cause the energy leakage. As for the isolation between the two input ports, which is a key characteristic requirement for dual-polarized antennas and arrays, the proposed array obtains a high value of 45 dB, which is much larger than those of the listed works. In addition, this array is fabricated by standard PCB technology, which is very cost-effective for mm-wave applications.

D. BEAM SCANNING PERFORMANCE

Beam scanning is a desired property for the future 5G applications. Although only a fixed-beam antenna array is demonstrated in this paper, the authors have considered the array's potential application of beam scanning by keeping the element space as compact as possible and suppressing the mutual coupling among elements as described in section II. So the presented array can also achieve beam scanning property by replacing the feed network with a conventional beamforming network such as the Rotman lens [22] and Butler matrix [25].

In this subsection, the beam scanning performance of the presented 1×8 array is further evaluated through the full wave simulation by HFSS. The 8-way feed networks are removed and all the eight elements are directly stimulated simultaneously. By setting a gradient phase distribution for the elements, the array can steer its beam in the xoy plane. The simulated results are shown in Figure 18. With the gain decreasing by 3 dB, the beam scans within +/−25 degree (i.e. phi ranges from 65 to 115 degree) for both V-pol and H-pol excitation, which proves the beam scanning ability of

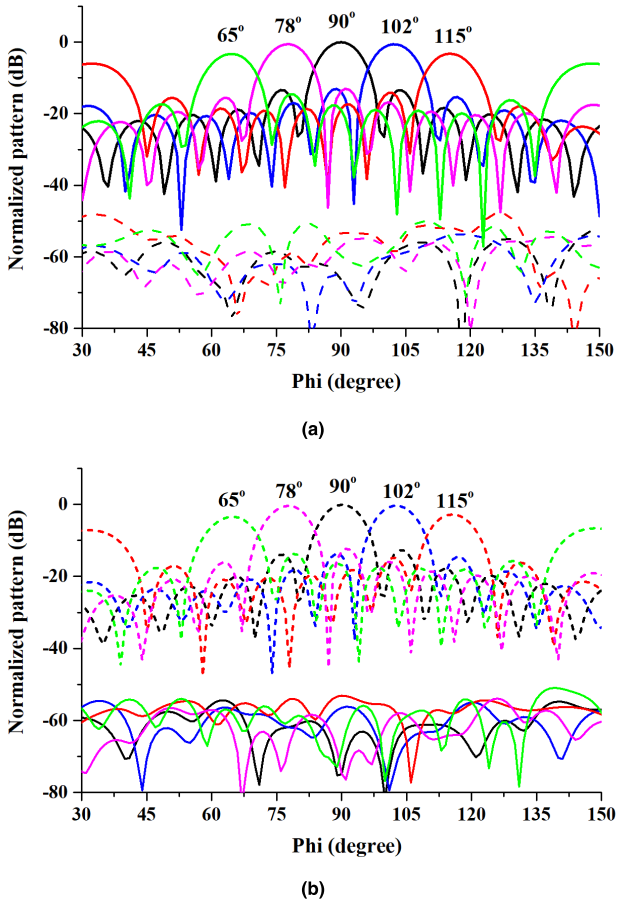

FIGURE 18. Simulated radiation patterns of beam scanning performance at 60 GHz: (a) V-pol excitation and (b) H-pol excitation.

the proposed antenna array although the grating lobe arises with the scanned angle increasing.

IV. CONCLUSION

A dual linearly polarized end-fire antenna array with a high isolation of 45 dB has been proposed and validated. The whole structure is integrated into four substrate layers and fabricated by cost-effective PCB technology. Bandwidths of 21% and 18% are achieved for the V-pol and H-pol operations respectively. Stable radiation patterns with cross polarizations below −30 dB and stable gains (peak gain of 16.1 dB for the V-pol and 15.1 dB for the H-pol) are obtained. The radiation efficiency is as stable as the gain and reaches a peak value of 82%. This design enlarges the family of dual-polarized end-fire antenna arrays and achieves many good performances therefore to be an attractive candidate to the future 5G applications.

ACKNOWLEDGEMENT

The authors would like to thank the anonymous reviewers for their useful comments and suggestions.

REFERENCES

[1] R. C. Daniels and R. W. Heath, "60 GHz wireless communications: Emerging requirements and design recommendations," *IEEE Veh. Technol. Mag.*, vol. 2, no. 3, pp. 41–50, Sep. 2007.

[2] M. S. Sharawi and M. Ikram, "Slot-based connected antenna arrays for 5G mobile terminals," in *Proc. Int. Workshop Antenna Technol. (iWAT)*, Nanjing, China, Mar. 2018, pp. 1–3.

[3] M. Ur-Rehman, N. A. Malik, X. Yang, Q. H. Abbasi, Z. Zhang, and N. Zhao, "A low profile antenna for millimeter-wave body-centric applications," *IEEE Trans. Antennas Propag.*, vol. 65, no. 12, pp. 6329–6337, Dec. 2017.

[4] K. Klionovski, A. Shamim, and M. S. Sharawi, "5G antenna array with wide-angle beam steering and dual linear polarizations," in *Proc. IEEE Int. Symp. Antennas Propag. USNC/URSI Nat. Radio Sci. Meeting*, Jul. 2017, pp. 1469–1470.

[5] J. F. Xu, Z. N. Chen, X. M. Qing, and W. Hong, "Bandwidth enhancement for a 60 GHz substrate integrated waveguide fed cavity array antenna on LTCC," *IEEE Trans. Antennas Progag.*, vol. 59, no. 3, pp. 826–832, Mar. 2011.

[6] Y. Miura, J. Hirokawa, M. Ando, Y. Shibuya, and G. Yoshida, "Double-layer full-corporate-feed hollow-waveguide slot array antenna in the 60-GHz band," *IEEE Trans. Antennas Propag.*, vol. 59, no. 8, pp. 2844–2851, Aug. 2011.

[7] S.-J. Park, D.-H. Shin, and S.-O. Park, "Low side-lobe substrate-integrated-waveguide antenna array using broadband unequal feeding network for millimeter-wave handset device," *IEEE Trans. Antennas Propag.*, vol. 64, no. 3, pp. 923–932, Mar. 2016.

[8] J. Wu, Y. J. Cheng, and Y. Fan, "Millimeter-wave wideband high-efficiency circularly polarized planar array antenna," *IEEE Trans. Antennas Propag.*, vol. 64, no. 2, pp. 535–542, Feb. 2016.

[9] Y. Li and K.-M. Luk, "A 60-GHz wideband circularly polarized aperture-coupled magneto-electric dipole antenna array," *IEEE Trans. Antennas Propag.*, vol. 64, no. 4, pp. 1325–1333, Apr. 2016.

[10] Q. Zhu, K.-B. Ng, and C. H. Chan, "Printed circularly polarized spiral antenna array for millimeter-wave applications," *IEEE Trans. Antennas Propag.*, vol. 65, no. 2, pp. 636–643, Feb. 2017.

[11] W. L. Stutzman and G. A. Thiele, *Antenna Theory and Design*. Hoboken, NJ, USA: Wiley, 2012.

[12] B. Y. E. Khatib, T. Djerafi, and K. Wu, "Three-dimensional architecture of substrate integrated waveguide feeder for Fermi tapered slot antenna array applications," *IEEE Trans. Antennas Propag.*, vol. 60, no. 10, pp. 4610–4618, Oct. 2012.

[13] Y. Yao, X. Cheng, C. Wang, J. Yu, and X. Chen, "Wideband circularly polarized antipodal curvedly tapered slot antenna array for 5G applications," *IEEE J. Sel. Areas Commun.*, vol. 35, no. 7, pp. 1539–1549, Jul. 2017.

[14] B. Yang, Z. Yu, Y. Dong, J. Zhou, and W. Hong, "Compact tapered slot antenna array for 5G millimeter-wave massive MIMO systems," *IEEE Trans. Antennas Propag.*, vol. 65, no. 12, pp. 6721–6727, Dec. 2017.

[15] W. Fang, P. Fei, and F. Nian, "Millimetre-wave end-fired antenna array for active 3D holographic imaging system," *Electron. Lett.*, vol. 50, no. 5, pp. 341–343, Feb. 2014.

[16] H. Chu and Y.-X. Guo, "A novel approach for millimeter-wave dielectric resonator antenna array designs by using the substrate integrated technology," *IEEE Trans. Antennas Propag.*, vol. 65, no. 2, pp. 909–914, Feb. 2017.

[17] Z. Chen, H. Liu, J. Yu, and X. Chen, "High gain, broadband and dual-polarized substrate integrated waveguide cavity-backed slot antenna array for 60 GHz band," *IEEE Access.*, vol. 6, pp. 31012–31022, 2018.

[18] D. Kim, M. Zhang, J. Hirokawa, and M. Ando, "Design and fabrication of a dual-polarization waveguide slot array antenna with high isolation and high antenna efficiency for the 60 GHz band," *IEEE Trans. Antennas Propag.*, vol. 62, no. 6, pp. 3019–3027, Jun. 2014.

[19] X.-L. Lu, H. Zhang, S.-M. Gu, H. Liu, X.-C. Wang, and W.-Z. Lu, "A dual-polarized cross-slot antenna array on a parallel-plate waveguide with compact structure and high efficiency," *IEEE Antennas Wireless Propag. Lett.*, vol. 17, no. 1, pp. 8–11, Jan. 2018.

[20] J. Xu, W. Hong, Z. H. Jiang, J. Chen, and H. Zhang, "A Q-band low-profile dual circularly polarized array antenna incorporating linearly polarized substrate integrated waveguide-fed patch subarrays," *IEEE Trans. Antennas Propag.*, vol. 65, no. 10, pp. 5200–5210, Oct. 2017.

[21] J. Zhu, S. Liao, Y. Yang, S. Li, and Q. Xue, "60 GHz dual-circularly polarized planar aperture antenna and array," *IEEE Trans. Antennas Propag.*, vol. 66, no. 2, pp. 1014–1019, Feb. 2018.
[22] L. Schulwitz and A. Mortazawi, "A compact dual-polarized multibeam phased-array architecture for millimeter-wave radar," *IEEE Trans. Microw. Theory Techn.*, vol. 53, no. 11, pp. 3588–3594, Nov. 2005.
[23] Y.-W. Hsu, T.-C. Huang, H.-S. Lin, and Y.-C. Lin, "Dual-polarized quasi Yagi–Uda antennas with endfire radiation for millimeter-wave MIMO terminals," *IEEE Trans. Antennas Propag.*, vol. 65, no. 12, pp. 6282–6289, Dec. 2017.
[24] Q. Wu, J. Hirokawa, J. Yin, C. Yu, H. Wang, and W. Hong, "Millimeter-wave multibeam endfire dual-circularly polarized antenna array for 5G wireless applications," *IEEE Trans. Antennas Propag.*, vol. 66, no. 9, pp. 4930–4935, Sep. 2018.
[25] Y. Li and K.-M. Luk, "60-GHz dual-polarized two-dimensional switch-beam wideband antenna array of aperture-coupled magneto-electric dipoles," *IEEE Trans. Antennas Propag.*, vol. 64, no. 2, pp. 554–563, Feb. 2016.
[26] Y. Zhao and K.-M. Luk, "Dual circular-polarized SIW-fed high-gain scalable antenna array for 60 GHz applications," *IEEE Trans. Antennas Propag.*, vol. 66, no. 3, pp. 1288–1298, Mar. 2018.
[27] Y. Li and K.-M. Luk, "A multibeam end-fire magnetoelectric dipole antenna array for millimeter-wave applications," *IEEE Trans. Antennas Propag.*, vol. 64, no. 7, pp. 2894–2904, Jul. 2016.
[28] J. Wang, Y. Li, L. Ge, J. Wang, and K.-M. Luk, "A 60 GHz horizontally polarized magnetoelectric dipole antenna array with 2-D multibeam endfire radiation," *IEEE Trans. Antennas Propag.*, vol. 65, no. 11, pp. 5837–5845, Nov. 2017.
[29] A. Li and K. M. Luk, "A dual-polarized magneto-electric dipole array for 60 GHz applications," in *Proc. Cross Strait Quad-Regional Radio Sci. Wireless Technol. Conf. (CSQRWC)*, Xuzhou, China, Jul. 2018, pp. 1–3.

AO LI was born in Sichuan, China, in 1993. He received the B.S. and M.S. degrees in electromagnetic field and microwave technology from the Harbin Institute of Technology, Harbin, China, in 2015 and 2017, respectively. He is currently pursuing the Ph.D. degree with the City University of Hong Kong. His research interests focus on millimeter wave antennas and arrays.

KWAI-MAN LUK (M'79–SM'94–F'03) was born in Hong Kong. He received the B.Sc. (Eng.) and Ph.D. degrees in electrical engineering from The University of Hong Kong, Hong Kong, in 1981 and 1985, respectively. He joined the Department of Electronic Engineering, City University of Hong Kong, Hong Kong, in 1985, as a Lecturer. Two years later, he was with the Department of Electronic Engineering, The Chinese University of Hong Kong, Hong Kong. In 1992, he returned to the City University of Hong Kong, where he was the Head of the Department of Electronic Engineering from 2004 to 2010 and the Director of the State Key Laboratory of Millimeter Waves from 2008 to 2013. He is currently the Chair Professor of electronic engineering with the City University of Hong Kong. He has authored four books, 10 research book chapters, over 350 journal papers, and 250 conference papers. He holds nine U.S. and more than 10 PRC patents. His current research interests include the design of patch antennas, magneto-electric dipole antennas, dense dielectric patch antennas, and open resonator antennas for various wireless applications. He was the Technical Program Chair of the 1997 Progress in Electromagnetics Research Symposium, the General Vice Chair of the 1997 and 2008 Asia Pacific Microwave Conference, the General Chair of the 2006 IEEE Region Ten Conference, the Technical Program Co-Chair of the 2008 International Symposium on Antennas and Propagation, and the General Co-Chair of the 2011 IEEE International Workshop on Antenna Technology, the 2014 IEEE International Conference on Antenna Measurements and Applications, and the 2015 International Conference on Infrared, Millimeter, and Terahertz Waves. He was a recipient of the Japan Microwave Prize at the 1994 Asia Pacific Microwave Conference in Chiba, the 2000 Croucher Foundation Senior Research Fellow in Hong Kong, the Best Paper Award at the 2008 International Symposium on Antennas and Propagation in Taipei, the 2011 State Technological Invention Award (Second Honor) of China, the Best Paper Award at the 2015 Asia-Pacific Conference on Antennas and Propagation in Bali, and the 2017 IEEE APS John Kraus Antenna Award.

He is a fellow of the Chinese Institute of Electronics, China, the Institution of Engineering and Technology, U.K., and the Electromagnetics Academy, USA. He was a Chief Guest Editor for the special issue on Antennas in Wireless Communications published in the PROCEEDINGS OF THE IEEE in 2012. He is currently the Deputy Editor-in-Chief of the PIERS journals and an Associate Editor of *IET Microwaves, Antennas and Propagation*.

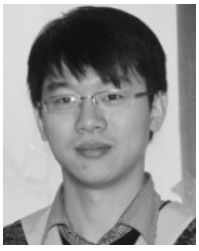

YUJIAN LI (S'12–M'15) was born in Hunan, China, in 1987. He received the B.S. and M.S. degrees in communications engineering from Beijing Jiaotong University, Beijing, China, in 2009 and 2012, respectively, and the Ph.D. degree in electronic engineering from the City University of Hong Kong in 2015.

He joined the Institute of Lightwave Technology, Beijing Jiaotong University, in 2015, as an Associate Professor. His current research interests include millimeter wave antennas, base station antennas, and leaky wave structures.

Dr. Li received the Outstanding Research Thesis Award from the City University of Hong Kong in 2015. He also received the Best Paper Award at the 2015 IEEE Asia-Pacific Conference on Antennas and Propagation, the Best Student Paper at the 2013 National Conference on Antennas, and the Best Student Paper Award (second prize) at the 2013 IEEE International Workshop on Electromagnetics (iWEM). He was selected as a Finalist in the Student Paper Contest of the 2015 IEEE AP-S Symposium on Antennas and Propagation. He has served as a Reviewer for the IEEE TRANSACTIONS ON ANTENNAS AND PROPAGATION, the IEEE ANTENNAS AND WIRELESS PROPAGATION LETTERS, and the *IET Microwaves, Antennas & Propagation*.